Available online at www.sciencedirect.com
SCIENCE DIRECT®
Combustion and Flame 142 (2005) 266–275
Combustion and Flame
www.elsevier.com/locate/combustflame

An experimental and modeling study of iso-octane ignition delay times under homogeneous charge compression ignition conditions

X. He, M.T. Donovan, B.T. Zigler, T.R. Palmer, S.M. Walton, M.S. Wooldridge *, A. Atreya

Department of Mechanical Engineering, University of Michigan, 2350 Hayward Street, Ann Arbor, MI 48109-2125, USA

Received 12 April 2004; received in revised form 20 January 2005; accepted 2 February 2005

Available online 3 May 2005

Abstract

Autoignition of iso-octane was examined using a rapid compression facility (RCF) with iso-octane, oxygen, nitrogen, and argon mixtures. The effects of typical homogeneous charge compression ignition (HCCI) conditions on the iso-octane ignition characteristics were studied. Experimental results for ignition delay times, τ_{ign}, were obtained from pressure time-histories. The experiments were conducted over a range of equivalence ratios ($\phi =$ 0.25–1.0), pressures ($P = 5.12$–23 atm), temperatures ($T = 943$–1027 K), and oxygen mole fractions ($\chi_{O_2} =$ 9–21%), and with the addition of trace amounts of combustion product gases (CO_2 and H_2O). It was found that the ignition delay times were well represented by the expression

$$\tau_{ign} = 1.3 \times 10^{-4} P^{-1.05} \phi^{-0.77} \chi_{O_2}^{-1.41} \exp(33{,}700/R_{(cal/mol/K)}T),$$

where P is pressure (atm), T is temperature (K), ϕ is the equivalence ratio (based on iso-octane to O_2 molar ratios), χ_{O_2} is the oxygen mole percent (%), and τ_{ign} is the ignition delay time (ms). Carbon dioxide was found to have no chemical effect on τ_{ign}. Water was found to systematically decrease τ_{ign} by a small amount (less than 14% for the range of conditions studied). The maximum uncertainty in the measured τ_{ign} is $\pm 12\%$ with an average uncertainty of $\pm 6\%$. The performance of several proposed chemical reaction mechanisms (including detailed, reduced, and skeletal mechanisms) was evaluated in the context of the current experimental results.

Keywords: Iso-octane; Ignition delay time; HCCI; Rapid compression facility

1. Introduction

Homogeneous charge compression ignition (HCCI) represents a potential major advance in high-efficiency, low-emission engines [1]. HCCI is lean burning and has no throttling losses, which leads to high efficiencies and low NO_x emissions (and, potentially, low particulate emissions) [1]. In addition, the

* Corresponding author. Fax: +1 734 647 3170.
E-mail address: mswool@engin.umich.edu (M.S. Wooldridge).

0010-2180/$ – see front matter
doi:10.1016/j.combustflame.2005.02.014

HCCI engine can have a much higher partial load efficiency than a spark ignition (SI) engine [2]. Although HCCI engines have been demonstrated to function well under some operating conditions, obstacles have been encountered in controlling the autoignition event over a large range of engine load and speed conditions, e.g., under low-load conditions, in cold starts, and during transients between operating conditions [1,3]. HCCI combustion is achieved by controlling the temperature, composition, and pressure of the fuel and air mixture so that it spontaneously ignites at or close to top dead center. Consequently, the control system is fundamentally more challenging than using a spark plug or fuel injector to determine ignition timing. It is generally well accepted that the local reaction kinetics are the most important processes affecting HCCI combustion [1]. Therefore, an extensive understanding of HCCI reaction chemistry is required to address technological barriers and develop valuable control strategies for HCCI engines.

The study of ignition delay times (τ_{ign}) of iso-octane (i-C_8H_{18}) mixtures is of particular interest because iso-octane is one of the primary reference fuels that determine octane numbers and knocking tendencies of gasoline mixtures under spark ignition operating conditions, and chemical kinetics of engine knock are very similar to kinetics of ignition under HCCI conditions. In addition, ignition delay time data provide valuable benchmark results for validation and refinement of the chemical reaction mechanisms used in many HCCI design tools and combustion simulations. Numerous detailed, skeletal, and reduced chemical reaction mechanisms have been developed in recent years to model HCCI combustion systems. These models require extensive validation, especially under conditions typical of anticipated HCCI operation.

Previous experimental studies of iso-octane ignition delay times have focused primarily on stoichiometric conditions, high temperatures, and moderate pressures (see, for example, the shock tube studies of Davidson et al. [4] and Vermeer et al. [5]). These studies provide valuable insight into the physical and chemical mechanisms important under conditions relevant to gasoline SI engines. However, there is a paucity of iso-octane ignition delay time data that have been obtained under HCCI conditions (e.g., $\phi < 1.0$; for example, see the shock tube study by Fieweger et al. [6] and the rapid compression machine studies by Minetti et al. [7] and Tanaka et al. [8]). Considerable uncertainty exists in extrapolating τ_{ign} to conditions beyond the experimental bounds of the studies. As high pressures, lean mixtures, relatively low temperatures ($T < 1100$ K), and the use of exhaust gases (via recirculation or internal residual gases) to affect ignition delay times are of interest for HCCI engine applications, additional data for τ_{ign} are needed for these conditions.

Thus, the objectives of this work are to determine the effects of P, T, and mixture composition, within the range of HCCI operating conditions, on τ_{ign} for iso-octane. To achieve these objectives, experiments over a broad range of state conditions using the free-piston rapid-compression facility (RCF) at the University of Michigan (UM) have been conducted. The results generated will provide much needed benchmark data for HCCI engine development and validation of proposed chemical reaction mechanisms.

2. Experimental approach

All ignition delay times were measured using the UM-RCF. A detailed description of the UM-RCF, the operating procedure, and the results of benchmark experimental studies characterizing its performance can be found in Donovan et al. [9], He et al. [10], and Donovan [11]. A schematic of the UM-RCF is shown in Fig. 1. Briefly, the UM-RCF consists of five major components—the driver section, the driven section, the test manifold, the sabot (i.e., free piston), and the hydraulic control valve assembly—and, in its most basic form, can be described as a simple piston–cylinder device. The driver section (154-mm i.d.) acts as a reservoir for high-pressure gases used to operate the UM-RCF and is connected to the driven section by a fast-acting globe valve. The driven section is the cylinder (2.74 m long, 101.2-mm i.d.) through which the sabot travels during operation (the sabot is loaded into the globe valve end of the driven section) and is

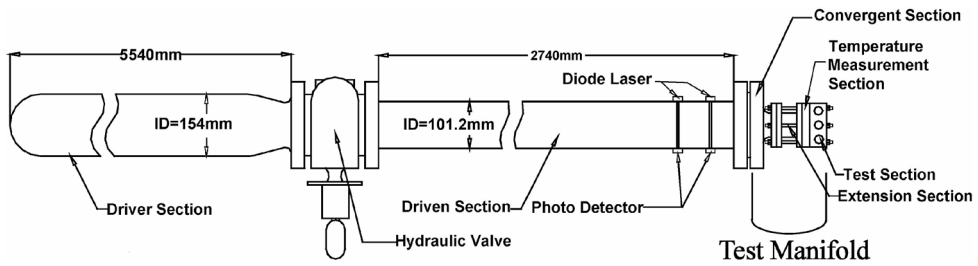

Fig. 1. Schematic of the University of Michigan rapid compression facility.

connected to the test manifold at its other end. Test gases are loaded into the middle of the driven section prior to operating the UM-RCF. During operation, the globe valve is opened (using the hydraulic control valve assembly), permitting the high-pressure driver gas to enter the driven section and rapidly accelerate the sabot. The test gas mixture in the driven section is compressed in front of the sabot and sealed within the test manifold.

The test manifold consists of components that permit control of the overall length of the manifold (extension sections) and that contain the various diagnostics available with the UM-RCF (thermocouple manifolds and the test section). Two extension sections are available in addition to the other components described in Donovan et al. [9]. The overall length of the test manifold can be used to control the overall compression ratio and, thereby, the end-of-compression gas temperatures. The length of the test manifold is set before each experiment and the test section is connected to the driven section using a stainless-steel convergent section that bridges the 101.2-mm bore of the driven section with the 50.8-mm bore of the remainder of the test manifold components. The polycarbonate thermocouple manifolds are designed for the mounting of fine wire thermocouples (Omega Engineering P10R-001, coated with thin layer of SiO_2 to prevent catalytic reaction on the thermocouple surface) across the bore of the test manifold and were used to obtain quantitative temperature measurements at various locations, both axially and radially, within the test manifold. The test section is equipped with two optical ports, a pressure transducer port, two additional instrumentation ports, and a gas inlet/outlet port. An end wall (either transparent for optical imaging or stainless steel) seals the test manifold. For the current study, the test section was instrumented with two photodiode detectors (Hamamatsu S1787-12 and Perkin–Elmer HUV-1100BQ/G) to monitor the visible and UV emission, and a piezoelectric transducer (Kistler 6041AX4) and charge amplifier (Kistler 5010B) for pressure measurements.

All test gas mixtures, with the exception of mixtures containing water vapor, were made using a dedicated mixing tank. Ultra-high purity grade nitrogen (99.998%) and oxygen (99.98%), prepurified argon (99.998%), carbon dioxide (99.8%, <50 ppm H_2O), distilled water, and iso-octane (>99.8%, 2,2,4-trimethylpentane, Aldrich) were used. The partial pressures of the mixture components were used to determine the mixture composition. To minimize the potential for fuel condensation, the maximum partial pressure of the iso-octane in the mixing tank was limited to <60% of the room-temperature vapor pressure of iso-octane.

For the H_2O experiments, a different test gas mixture preparation strategy was used. An i-$C_8H_8/Ar/N_2/O_2$ mixture with the desired equivalence ratio and dilution level was made in the dedicated mixing tank. Water vapor was directed into a second large mixing tank. The H_2O and i-$C_8H_8/Ar/N_2/O_2$ mixture were then charged from the middle into the driven section and allowed to mix for ~30 min prior to conducting each experiment. Although pure diffusion times may indicate a need for mixing times of ~2.6 h (based on initial charge pressures of ~0.2 atm, $T = 298$ K, H_2O diffusing into N_2, and a diffusion length of 1.37 m), the 30-min mixing time was considered sufficient to achieve homogeneous mixtures in the test section for the following reasons. The i-$C_8H_8/Ar/N_2/O_2$ mixtures are charged into the RCF at high pressures (relative to the pressure in the driven section of the RCF); therefore, the injection velocity of the gases entering the RCF accelerates the mixing process. In addition, the compression of the test gases during each experiment induces motion (and commensurate mixing) of the test gas mixtures. Thus, mixture inhomogenieties are not sustained after compression. This conclusion is supported by high-speed imaging, which shows nearly uniform emission throughout the test volume under the H_2O conditions studied. Leakage of room air into the UM-RCF during the mixing period amounted to less than 0.2% of the total test gas volume and is accounted for in the mixture compositions reported.

Throughout the current study, argon was used as a balance gas to ensure the heat capacities of the mixtures were approximately constant for all experiments. Thus, each mixture yields the same temperatures at the end of compression if the compression ratios for the experiments are the same, and the effects of heat capacity on the τ_{ign} are eliminated.

3. Experimental results

Fig. 2 presents typical experimental results of pressure, UV, and visible emission time histories for conditions of $\phi = 0.4$ (0.67% iso-octane, 20.9% O_2, 14.8% Ar, and 63.63% N_2). In this work, the equivalence ratio is defined as

$$\phi \equiv \frac{(\chi_{i-C_8H_{18}}/\chi_{O_2})}{(\chi_{i-C_8H_{18}}/\chi_{O_2})_{stoichiometric}},$$

and all compositional fractions are mole fractions. Note that high-frequency (>2.5 kHz) disturbances generated by the impact of the free piston are filtered from the pressure time-histories. All data exhibit the same general features seen in Fig. 2, where the compression process leads to a smooth, continuous increase in pressure. The bulk (~85%) of the pressure rise due to compression occurs in a short time

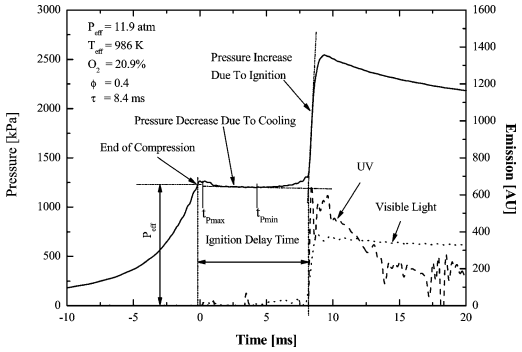

Fig. 2. Illustration of method used to determine ignition delay times from pressure–time histories and typical data.

(<10 ms). The first pressure maximum occurs as a result of compression and sealing of the gases in the test section. This peak is followed by a decrease in pressure due to heat losses to the test section walls, followed by an increase in pressure due to ignition, resulting in a second maximum. Note, time $t = 0$ s corresponds to the first peak in the pressure time-history. The UV and visible emission signals provide additional indications of ignition and, as seen in Fig. 2, track closely with the pressure time-histories.

Although thermocouple-measured temperature time-histories were obtained for the majority of the experiments conducted, the thermocouple data were not used for correlating the ignition delay times due to the uncertainties associated with the interpretation of the thermocouple data. These uncertainties are due predominantly to the transient nature of the thermocouple time constant during the compression and ignition processes (both the gas velocity across the thermocouple bead and the gas properties are time-varying). However, thermocouple data were used to prove the existence of an isentropic core region of gases of approximately uniform conditions during nonreactive, inert gas experiments. It is important to prove the existence of a core region because gases in this region undergo an isentropic compression process that forms the basis of the present data analysis. Further details on the inert gas characterization studies are provided in Donovan et al. [9].

The ignition delay time for each experiment was obtained from the pressure time-histories in the following manner. First, an effective pressure (P_{eff}) was defined as the integrated average pressure from the maximum pressure (due to compression) to the minimum pressure (due to cooling) after compression, but before ignition:

$$P_{\mathrm{eff}} = \frac{1}{(t_{P_{\mathrm{min}}} - t_{P_{\mathrm{max}}})} \int_{t_{P_{\mathrm{max}}}}^{t_{P_{\mathrm{min}}}} P\,dt. \tag{1}$$

The effective temperature (T_{eff}) was then calculated from P_{eff} and the initial temperature (T_0, typically 298 K) and pressure (P_0, the charge pressure) by numerically integrating the isentropic relation

$$\int_{T_0}^{T_{\mathrm{eff}}} \frac{\gamma}{\gamma - 1}\, d\ln T = \ln\left(\frac{P_{\mathrm{eff}}}{P_0}\right), \tag{2}$$

where γ is the specific heat ratio of the test gas mixture. The ratio of the specific heats (γ) was determined from the NASA Thermodynamic Data Base [12].

The end of compression was designated at the first time the pressure reached P_{eff} due to compression (see Fig. 2). This point was used as the starting point for τ_{ign}. To determine the start of ignition from the pressure trace, the pressure time-history, which corresponds to the last stage of the pressure drop due to heat loss to the test section walls was linearly extrapolated. The portion of the pressure trace that corresponded to the sharp initial pressure rise due to ignition was also linearly extrapolated. The intersection of the two linear fits was designated the start of ignition. Fig. 2 shows an example of the methodology used to determine τ_{ign} from a typical pressure time-history. To verify the method used to determine τ_{ign}, a similar methodology was applied to the UV emission data. The agreement between the two approaches was excellent (within 5% for most cases). Note, in the remainder of the article, P and T are used interchangeably with P_{eff} and T_{eff}.

A summary of the iso-octane ignition delay time data is provided in Tables 1 and 2. Regression analysis was performed on the data, and the following correlation yielded excellent agreement with the experimental data ($R^2 = 0.98$):

$$\tau_{\mathrm{ign}} = 1.3 \times 10^{-4} P^{-1.05} \phi^{-0.77} \chi_{\mathrm{O_2}}^{-1.41} \times \exp(33{,}700/R_{(\mathrm{cal/mol/K})}T). \tag{3}$$

Here, P is pressure (atm), T is temperature (K), ϕ is the equivalence ratio, $\chi_{\mathrm{O_2}}$ is the oxygen mole percent (%), and τ_{ign} is the ignition delay time (ms). Figs. 3–5 summarize the effects of T, ϕ, and P on τ_{ign}, respectively, where the data (except Fig. 4) have been normalized as necessary using Eq. (3). In Fig. 5, the data are presented as a function of ϕ and $(\mathrm{N_2} + \mathrm{Ar})/\mathrm{O_2}$ ratio, and Eq. (3) is provided for comparison. Note that the different categories of data show no systematic deviations from Eq. (3).

As mentioned above, mixtures that included addition of H_2O or CO_2 to the initial reactants were investigated in the UM-RCF to determine the effects (if any) on the iso-octane ignition delay time. Possible effects of CO_2 and H_2O on τ_{ign} can be classified into two categories: physical effects (due to the large heat

Table 1
Summary of experimental results for mixtures containing no EGR gases[a]

Ar (%)	O_2 (%)	ϕ	P_{eff} (atm)	T_{eff} (K)	τ_{ign} (ms)
4.0	16.6	0.25	13.8	961	20.6
4.0	16.6	0.25	8.60	980	24.4
4.0	16.6	0.25	15.1	983	13.5
5.8	16.6	0.3	10.5	954	31.2
5.8	16.6	0.3	10.8	964	23.7
5.8	16.6	0.3	10.9	967	22.2
5.8	16.6	0.3	11.4	975	17.6
5.8	16.6	0.3	11.5	978	16.8
5.8	16.6	0.3	11.4	980	16.6
5.8	16.6	0.3	8.54	981	22.0
5.8	16.6	0.3	9.23	983	19.0
5.8	16.6	0.3	14.77	983	11.4
5.8	16.6	0.3	11.94	985	14.2
5.8	16.6	0.3	9.43	1003	12.7
5.8	16.6	0.3	8.86	1015	10.9
5.8	16.6	0.3	9.90	1015	10.0
5.8	16.6	0.3	9.97	1016	9.9
5.8	16.6	0.3	8.96	1019	10.3
7.8	16.6	0.35	14.1	969	13.8
7.8	16.6	0.35	14.3	971	13.2
10.0	16.6	0.4	13.7	945	20.5
10.0	16.6	0.4	10.3	950	24.3
10.0	16.6	0.4	13.8	953	16.0
10.0	16.6	0.4	10.5	956	21.7
10.0	16.6	0.4	11.3	961	19.8
10.0	16.6	0.4	14.2	962	13.8
14.7	20.9	0.4	21.5	968	5.6
10.0	16.6	0.4	9.72	969	19.7
10.0	16.6	0.4	15.1	975	10.0
10.0	20.9	0.4	17.8	977	6.5
10.0	20.9	0.4	17.9	978	6.3
10.0	16.6	0.4	11.1	978	14.1
10.0	16.6	0.4	8.88	982	17.2
14.7	20.9	0.4	15.5	983	6.9
10.0	16.6	0.4	15.5	984	8.4
10.0	16.6	0.4	16.2	985	8.6
14.7	20.9	0.4	11.9	986	8.4
10.0	16.6	0.4	15.6	986	9.0
10.0	16.6	0.4	12.0	988	11.4
10.0	16.6	0.4	5.24	997	21.9
10.0	16.6	0.4	5.21	998	23.3
10.0	16.6	0.4	5.16	999	21.6
10.0	16.6	0.4	5.25	1001	21.1
10.0	16.6	0.4	5.30	1003	19.5
10.0	16.6	0.4	5.67	1004	17.4
10.0	16.6	0.4	5.41	1004	18.7
10.0	16.6	0.4	5.40	1004	18.9
10.0	16.6	0.4	5.36	1006	17.8
10.0	16.6	0.4	5.44	1008	17.6
10.0	16.6	0.4	5.38	1008	17.7
10.0	16.6	0.4	5.12	1010	18.3
10.0	16.6	0.4	5.35	1016	16.2
10.0	16.6	0.4	5.28	1019	14.6
10.0	16.6	0.4	5.37	1022	13.8
10.0	16.6	0.4	6.47	1025	11.2
10.0	16.6	0.4	6.81	1027	10.4
14.0	16.6	0.5	10.3	953	21.6
14.0	16.6	0.5	10.4	954	19.9
14.0	16.6	0.5	10.6	959	16.3
14.0	16.6	0.5	20.8	960	8.9
14.0	16.6	0.5	10.7	964	16.5
14.0	16.6	0.5	11.1	966	15.7
14.0	16.6	0.5	11.2	969	14.2
14.0	16.6	0.5	11.0	971	13.8
14.0	16.6	0.5	11.4	978	12.2
14.0	16.6	0.5	18.2	981	7.1
14.0	16.6	0.5	15.8	988	7.3
17.9	16.6	0.6	10.9	943	18.4
17.9	16.6	0.6	11.1	948	16.4
17.9	16.6	0.6	11.0	969	12.1
17.9	16.6	0.6	11.1	975	11.1
17.9	16.6	0.6	17.9	977	6.3
17.9	16.6	0.6	8.64	982	13.0
17.9	16.6	0.6	11.7	983	8.9
17.9	16.6	0.6	15.6	984	6.3
17.9	16.6	0.6	23.1	986	4.1
17.9	16.6	0.6	8.83	987	11.6
21.9	16.5	0.7	17.8	976	5.1
21.9	16.5	0.7	15.4	982	5.6
25.7	16.6	0.8	8.72	983	9.0
25.7	16.6	0.8	8.83	987	9.0
14.5	9.1	1.0	15.5	943	19.9
14.5	9.1	1.0	17.9	977	10.3
14.5	9.1	1.0	11.6	981	15.3
21.3	11.7	1.0	15.5	984	7.0
14.5	9.1	1.0	15.5	984	10.4
21.3	11.7	1.0	18.5	985	6
33.5	16.6	1.0	8.81	986	7.1

[a] Composition data are provided on a mole basis. All experiments were conducted using N_2 as the balance gas. The equivalence ratio is based on iso-octane-to-O_2 molar ratios.

capacities of these molecules) and chemical effects. The physical effect can be determined by simply investigating the effect of temperature on τ_{ign}. In the current work, possible changes in the reaction chemistry that might occur due to the presence of CO_2 and H_2O were of interest. Here, argon was used to control the heat capacity of the mixture to target temperatures in the same range as the other UM-RCF iso-octane experiments. The results for the CO_2 experiments are listed in Table 2. Carbon dioxide additions of 0.5, 2.0, and 3.0% (mole basis) were examined. The mixture mole fractions for H_2O and CO_2 were selected based on anticipated levels of exhaust gases for use in HCCI systems. Comparison of the CO_2 results with baseline data for τ_{ign} obtained under similar conditions with no CO_2 in the reactant mixtures indicates that CO_2 does not appear to have a chemical effect on τ_{ign} under the conditions studied.

The results for addition of 3% H_2O (mole basis) are shown in Fig. 6 and listed in Table 2. The cor-

Table 2
Summary of experimental results for mixtures containing CO_2 or H_2O

CO_2[a] (%)	H_2O[a] (%)	Ar (%)	P_{eff} (atm)	T_{eff} (K)	τ_{ign} (ms)
3.0	–	15.0	11.7	982	11.5
3.0	–	15.0	15.4	982	8.7
3.0	–	15.0	16.0	951	14.2
3.0	–	15.0	22.7	982	5.3
0.5	–	11.7	11.8	989	10.3
0.5	–	11.7	15.5	984	8.1
0.5	–	11.7	18.3	986	6.9
0.5	–	11.7	20.7	962	9.1
2.0	–	13.3	11.2	975	13.9
2.0	–	13.3	13.8	955	16.0
2.0	–	13.3	17.8	975	8.3
2.0	–	13.3	21.2	965	8.2
–	3.0	11.9	11.7	979	12.9
–	3.0	11.9	13.7	949	17.4
–	3.0	11.9	15.4	973	10.0
–	3.0	11.9	16.8	950	13.3
–	3.0	11.9	14.8	969	10.6
–	3.0	11.9	14.0	954	15.0
–	3.0	11.9	13.0	955	14.7
–	3.0	11.9	14.7	967	11.3

[a] All experiments were conducted using an equivalence ratio of $\phi = 0.4$ and O_2 mole fraction, χ_{O_2} of 16.6%, and using N_2 as the balance gas.

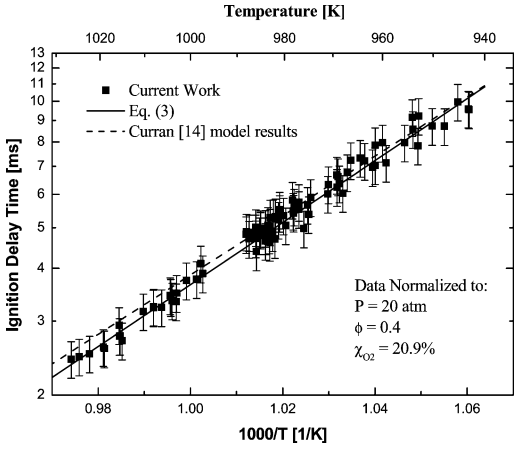

Fig. 3. Summary of results for iso-octane ignition delay times. The error bars denote the uncertainty in the measurements.

relation for the baseline data with no water addition (Eq. (3)) is included in Fig. 6 for comparison. Unlike CO_2, water seems to have a slight chemical effect on τ_{ign}. On average, the mixtures including H_2O addition exhibited lower ignition delay times. These results are discussed further below.

An extensive error analysis was conducted to quantify the uncertainty in the results of the current

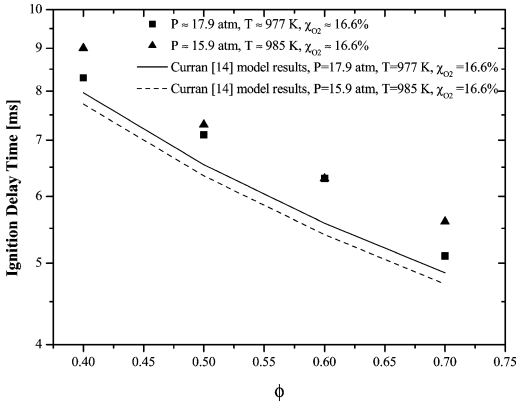

Fig. 4. Influence of equivalence ratio on τ_{ign}.

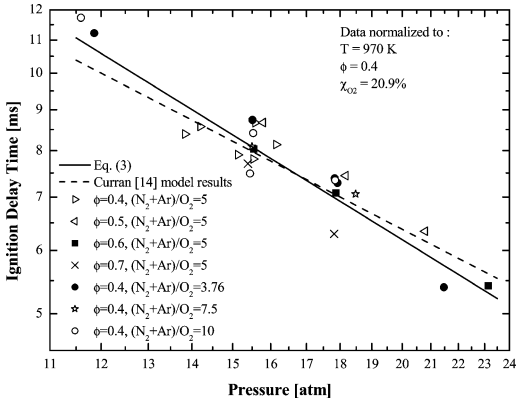

Fig. 5. Influence of pressure on τ_{ign}.

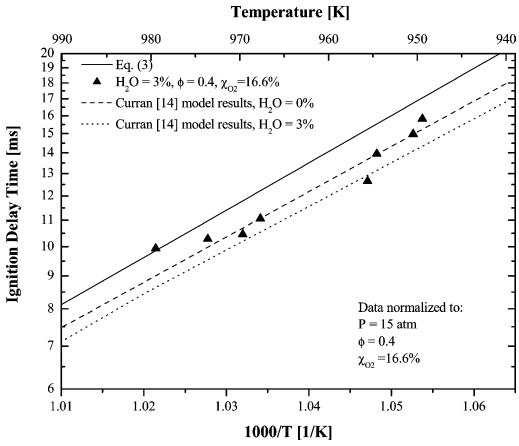

Fig. 6. Influence of H_2O on τ_{ign}.

study. The primary sources of uncertainty in τ_{ign} are due to uncertainties in the mixture composition (which yields an uncertainty of 0.65% in the determination of the mixture equivalence ratio and the mole fraction of O_2), uncertainties in the pressure measure-

ment (which are due primarily to the definition of the effective pressure and the accuracy of the pressure transducer and charge amplifier), and corresponding uncertainties in the calculated effective temperature. Combining the results of the uncertainty analysis, the uncertainty of the ignition delay time is determined for each experiment using the equation

$$\Delta\tau_{\text{ign}} = \left(\left(\frac{\partial \tau_{\text{ign}}}{\partial T} dT \right)^2 + \left(\frac{\partial \tau_{\text{ign}}}{\partial P} dP \right)^2 + \left(\frac{\partial \tau_{\text{ign}}}{\partial \chi_{O_2}} d\chi_{O_2} \right)^2 + \left(\frac{\partial \tau_{\text{ign}}}{\partial \phi} d\phi \right)^2 \right)^{1/2}, \quad (4)$$

where the partial differential coefficients are calculated based on Eq. (3). The error bars in Fig. 3 represent the results of the uncertainty analysis. The maximum uncertainty of the current study is ±12%, and the average uncertainty ±6%.

4. Discussion

In Fig. 7, the results of the current work are compared with results of previous shock tube and RCF studies of iso-octane ignition delay times. Here, all data have been normalized to $P = 20$ atm, $\phi = 0.4$, and $\chi_{O_2} = 20.9\%$ using Eq. (3). As seen in Fig. 7, the current work is in very good agreement with the low-temperature shock tube study by Fieweger et al. [6] and the more recent low-temperature shock tube study by Davidson et al. [13]. Compared with the ignition delay times in the relatively high temperature ($T > 900$ K) region, the experimental results for τ_{ign} show much larger scatter as temperature approaches the negative temperature coefficient (NTC) region ($T < 850$ K). This may be due to uncertainties in the gas temperatures due to the long test times required at these low temperatures. Note that knowledge of the functional dependence of τ_{ign} on ϕ is critical for accurate determination of the activation energy. As seen in Fig. 7, only few data under fuel-lean conditions existed for τ_{ign} prior to this study. In addition, inert gases are used (in part) to control temperature in both RCF and shock tube studies. Understanding the effects of dilution on τ_{ign} (presented here as the functional dependence on χ_{O_2}) is therefore also important.

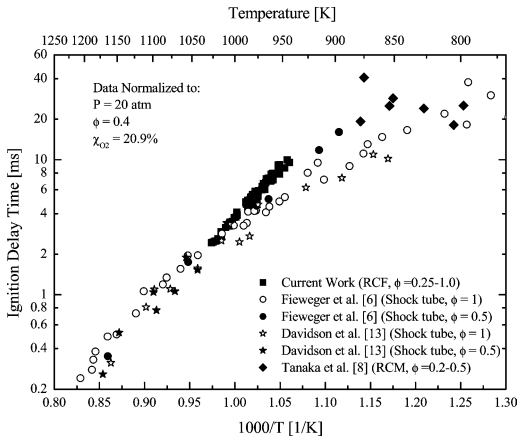

Fig. 7. Comparison of current results for iso-octane ignition delay times with those for previous shock tube and RCF studies.

As shown in Eq. (3), an overall activation energy (E_a) of 33.7 kcal/mol was determined in the course of this work. The value for E_a is lower than the activation energy of 43.9 kcal/mol reported by Davidson et al. [4] for high-temperature iso-octane ignition delay time studies. The difference in E_a for the two temperature regimes is likely due to the increased role of the carbonyl-hydroperoxide species on reaction kinetics at these relatively low temperatures. This is discussed further below.

Similarly, the pressure dependence and equivalence ratio dependence observed in the current study differ from previous results obtained at higher temperatures. For example, Davidson et al. [4] found $\tau_{\text{ign}} \propto P^{-0.56}$ for shock tube experiments with i-C_8H_{18}/O_2/Ar mixtures at $T = 1117$–2009 K. They also found that τ_{ign} increased with increasing ϕ according to $\tau_{\text{ign}} \propto \phi^{1.62}$.

To better understand the effects of P, T, ϕ, and χ_{O_2} on low-temperature iso-octane ignition, CHEMKIN modeling of the RCF experiments was conducted using the detailed reaction mechanism of Curran et al. [14]. For the modeling studies, the Aurora/Chemkin 3.7.1 suite of programs [15] was used. Two modeling approaches were investigated. The first model simulated the compression process and the expansion of the core gases after compression. The second model was more simplified and considered the post-compression conditions as an adiabatic, constant-volume system.

In Model 1, the initial charge pressure, temperature, and reactant composition were used as the initial conditions of the Chemkin calculation. An adiabatic process with constant internal energy was assumed, and a volume time-history that includes both the compression and postcompression processes was used in the model. By including the volume change in the Chemkin calculation, the model simulates the actual compression and ignition processes of the core gas mixture. The volume time-history used in the model was obtained in the following manner. The pressure time-history was divided into two time intervals: compression and post-compression. During compression, changes in pressure and temperature due to chemi-

cal reaction are small (although some reaction does occur in the final stages of compression). Isentropic compression was assumed, and a polynomial fit was applied to the experimental pressure trace to calculate the volume change during compression. After compression, the test gas in the core region undergoes a slight expansion (due to heat losses to the chamber walls). To obtain the expansion rate of the core gases in the test section (or, in other words, estimate the effects of the heat losses on the volume of the adiabatic core region of the test gases), inert gas experiments were conducted under experimental conditions comparable to those for the iso-octane ignition studies. The pressure trace of the inert gas experiments after compression was then used to calculate the volume expansion of the core gas, again assuming an isentropic process.

For Model 2, a constant-volume, adiabatic process is assumed where the initial conditions are the effective temperature, the effective pressure, and the initial test gas composition. Model 2 does not include the effects of reaction during compression. The same reaction mechanism and thermodynamic data were used for each model.

As seen in Fig. 8, the two modeling approaches yield very similar results for the ignition delay time, with a difference of less than 5%. Based on the good agreement between the two modeling approaches, the definitions used in this work for effective temperature and effective pressure were considered a good basis for input conditions for zero-dimensional modeling, and the simplified Model 2 approach was considered adequate for evaluation of modeling trends.

The Model 2 results using the Curran et al. [14] mechanism are included in Figs. 3–6. In general, the modeling results using this mechanism were in good agreement with the experimental results, particularly in terms of activation energy ($E_{a,\mathrm{Curran}} = 32.3$ kcal/mol vs $E_{a,\mathrm{experimental}} = 33.7$ kcal/mol)

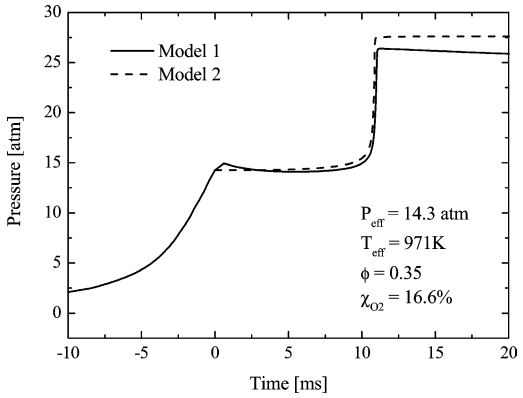

Fig. 8. Comparison of chemical kinetic modeling approaches.

and dependence on ϕ. In the extensive modeling study conducted by Curran et al. [14], the authors found that at temperatures below 1150 K, fuel-lean mixtures ignite more slowly than fuel-rich mixtures. This trend was attributed to the production of carbonyl-hydroperoxide species which lead to chain branching. The production of carbonyl-hydroperoxide species is directly proportional to the fuel concentration; thus, increasing ϕ leads to increased radical production and decreased ignition delay times [14]. At temperatures above 1150 K, the key $H + O_2 \rightarrow OH + O$ branching reaction becomes more important, and increasing the O_2 concentration decreases the ignition delay time. As seen in Fig. 4, the experimental results of the current study confirm that τ_{ign} increases with decreasing equivalence ratio. The data shown in Fig. 4 have not been normalized, and although the temperature and pressure for each data point are not exactly the same, the results clearly indicate the strong effect of ϕ on τ_{ign}.

The Curran et al. [14] mechanism predicts a weaker dependence of pressure (see Fig. 5) and slightly shorter ignition delay time when 3% H_2O is added to a baseline reactant mixture (see Fig. 6). Note that the magnitude of the shift in τ_{ign} predicted to occur when water is added to the mixture is within the uncertainty in the experimental measurements. However, a decrease in τ_{ign} of 7.1% (on average) was observed in the experiments.

Many iso-octane combustion mechanisms have been developed in addition to the Curran et al. [14] mechanism. The performance of several other mechanisms at reproducing the UM-RCF iso-octane results was also evaluated. Table 3 lists the mechanisms considered and key features of the mechanisms. A summary of the predictions of the reaction mechanisms (Curran et al. [14], Golovichev/Chalmer University [16], Tanaka et al. [17], and Glaude et al. [18]) is presented as a function of temperature in Fig. 9. Values for E_a as determined from these results are provided in Table 3. All mechanisms are in relatively good agreement with the experimentally determined value for E_a. Similar comparisons between the modeling and the experimental results can be generated for ϕ, P, and χ_{O_2}. The results in terms of the other fitting parameters for τ_{ign} (using the form $\tau_{\mathrm{ign}} = AP^n\phi^m\chi_{O_2}^k \exp(E_a/R_{(\mathrm{cal/mol/K})}T)$ are also provided in Table 3, along with the conditions under which the evaluations were conducted. Although each mechanism demonstrates good performance in reproducing trends for some parameters, the results of the Curran et al. [14] model and the Golovichev/Chalmer University [16] model agree better both in absolute magnitude and in prediction of quantitative trends. The Curran et al. [14] model predicts a weaker influence of oxygen mole fraction on τ_{ign} ($k = -1.07$)

Table 3
Features and results of iso-octane chemical reaction mechanisms examined[a]

	Number of species	Number of reactions	Mechanism type	A	E_a (kcal/mol)	n	m	k
Current study	–	–	–	1.30E−4	33.7	−1.05	−0.77	−1.41
Curran et al. [14]	858	3606	Detailed	5.36E−5	32.3	−0.88	−0.88	−1.07
Golovichev/Chalmers University [16]	84	412	Skeletal	3.13E−4	30.4	−0.94	−0.84	−1.22
Tanaka et al. [17]	38	61	Reduced	1.28E−4	33.8	−1.01	−0.81	−1.73
Glaude et al. [18]	353	1481	Detailed	6.25E−4	28.8	−0.90	−0.64	−1.04

[a] The fitting parameters were derived for a function of the form $\tau_{ign} = AP^n\phi^m\chi_{O_2}^k \exp(E_a/R_{(cal/mol/K)}T)$.

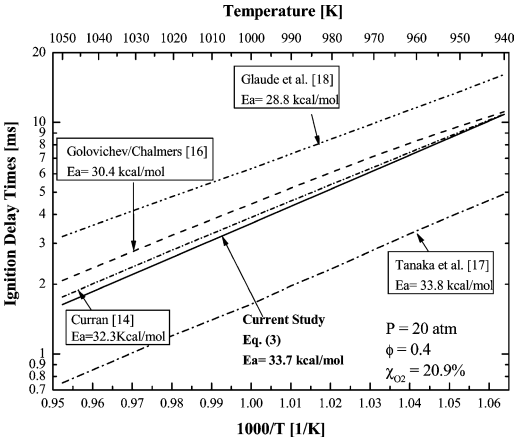

Fig. 9. Comparison of experimental and modeling results (calculated using different chemical reaction mechanisms) for the influence of temperature on iso-octane ignition delay times.

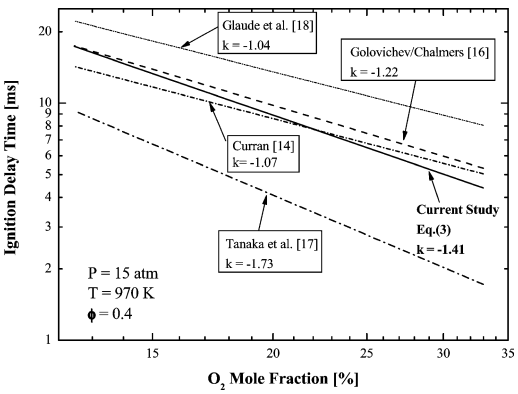

Fig. 10. Comparison of experimental and modeling results (calculated using different chemical reaction mechanisms) for the influence of oxygen mole fraction on iso-octane ignition delay times.

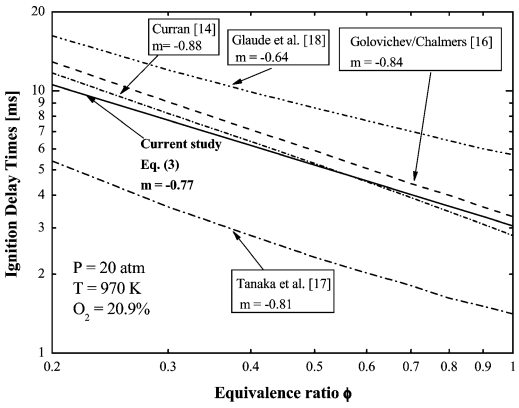

Fig. 11. Comparison of experimental and modeling results (calculated using different chemical reaction mechanisms) for the influence of equivalence ratio on iso-octane ignition delay times.

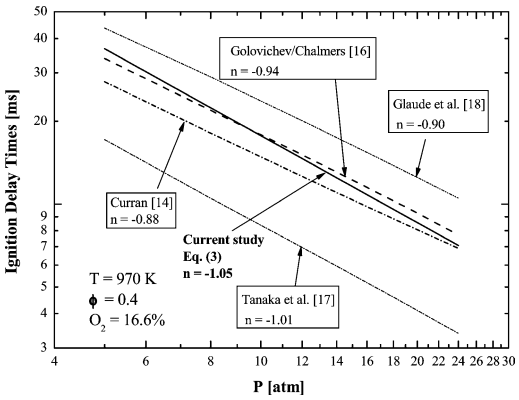

Fig. 12. Comparison of experimental and modeling results (calculated using different chemical reaction mechanisms) for the influence of pressure on iso-octane ignition delay times.

than the experimental results ($k = -1.41$). As can be seen in Fig. 10, the Curran model overpredicts τ_{ign} when χ_{O_2} is higher than 22%, and underpredicts τ_{ign} when χ_{O_2} is lower than 22%. The results of the Golovichev/Chalmers University [16] model ($k = -1.22$) show a similar tendency (see Fig. 10), where the model overpredicts τ_{ign} when χ_{O_2} is higher than 13% and underpredicts τ_{ign} when χ_{O_2} is less than 13%. The mechanism of Glaude et al. [18] consistently overpredicts τ_{ign} by ∼30%, and the mechanism by Tanaka et al. [17] consistently under predicts

τ_{ign} by ~60% under the conditions studied. However, the trends predicted by the Tanaka mechanism are in very good agreement with the experimental results, which is quite remarkable, given the level of empiricism incorporated into the model.

Similar comparisons of the modeling results are shown in Figs. 11 and 12 for τ_{ign} as a function of equivalence ratio and pressure, respectively. As expected, based on the data in Table 3, the models are in generally good agreement with the trends for ϕ and P, with varying levels of agreement with the absolute values for the ignition delay time. Note that the level of agreement on an absolute basis varies based on the normalization conditions selected.

5. Conclusions

These experiments have attempted to clarify the roles of temperature, pressure, equivalence ratio, diluent (Ar and N_2)-to-oxygen ratio, and EGR gases (CO_2 and H_2O) on ignition delay times of iso-octane mixtures under conditions relevant to HCCI operation. The results of this study are the first experimental data available for iso-octane ignition delay times at low temperature, high pressure, and low equivalence ratio conditions. The results reported for ignition delay time could not have been predicted using existing correlations or extrapolated from existing experimental data without considerable error/uncertainty. Thus, these new data have considerable potential for impact on the development of control strategies for HCCI engine technologies.

Specifically, τ_{ign} was found to be a strong function of ϕ, consistent with model predictions by Curran et al. [14], and demonstrated a functional relationship opposite to that observed at high temperatures. Similarly, the pressure dependence of τ_{ign} is stronger than that observed at higher temperatures. The experimental results were well represented by Eq. (3). In addition, using Eq. (3), where $\tau_{ign} \propto \phi^{-0.77}$, facilitated direct comparison of the current work with previous studies of iso-octane ignition conducted in other facilities at other conditions. The experimental data summarized in Fig. 6 are in very good agreement. The detailed mechanism developed by Curran et al. [14] showed exceptional performance at reproducing the experimental results when χ_{O_2} was close to 22%. The Golovichev/Chalmers University model performed similarly well when χ_{O_2} was close to 13%.

Acknowledgments

The authors acknowledge the generous support of the Department of Energy via the HCCI University Consortium. We also thank Professor Ronald Hanson and his research group at Stanford University for sharing their recent shock tube results.

References

[1] K. Epping, S. Aceves, R. Bechtold, J. Dec, The Potential of HCCI Combustion for High Efficiency and Low Emissions, 2002, SAE paper 2002-01-1923.
[2] M. Christensen, P. Einewall, B. Johansson, Homogeneous Charge Compression Ignition (HCCI) Using Isooctane, Ethanol and Natural Gas: A Comparison to Spark Ignition Operation, 1997, SAE paper 972874.
[3] A. Hultqvist, M. Christensen, B. Johansson, M. Richter, J. Nygren, J. Hult, M. Alden, The HCCI Combustion Process in a Single Cycle: High-Speed Fuel Tracer LIF and Chemiluminescence Imaging, 2002, SAE paper 2002-01-0424.
[4] D.F. Davidson, M.A. Oehlschlaeger, J.T. Herbon, R.K. Hanson, Proc. Combust. Inst. 29 (2002) 1295–1304.
[5] D.J. Vermeer, J.W. Meyer, A.K. Oppenheim, Combust. Flame 18 (1972) 327–336.
[6] K. Fieweger, R. Blumenthal, G. Adomeit, Combust. Flame 109 (1997) 599–619.
[7] R. Minetti, M. Carlier, M. Ribaucour, E. Therssen, L.R. Sochet, Proc. Combust. Inst. 26 (1996) 747–753.
[8] S. Tanaka, F. Ayala, J.C. Keck, J.B. Heywood, Combust. Flame 132 (2003) 219–239.
[9] M.T. Donovan, X. He, B.T. Zigler, T.R. Palmer, M.S. Wooldridge, A. Atreya, Combust. Flame 137 (2004) 351–365.
[10] X. He, M.T. Donovan, T.R. Palmer, B.T. Zigler, M.S. Wooldridge, A. Atreya, in: Proceedings of the Third Joint Meeting of the U.S. Sections of The Combustion Institute, March 16–19, 2003, pp. 1–6, paper B24.
[11] M.T. Donovan, Ph.D. dissertation, Department of Mechanical Engineering, University of Michigan, 2003.
[12] B.J. McBride, S. Gordon, M.A. Reno, NASA Technical Memorandum 4513, October 1993.
[13] D.F. Davidson, B.M. Gauthier, R.K. Hanson, Proc. Combust. Inst. 30 (2004) PID 28621.
[14] H.J. Curran, P. Gaffuri, W.J. Pitz, C.K. Westbrook, Combust. Flame 129 (2002) 253–280.
[15] R.J. Kee, F.M. Rupley, J.A. Miller, M.E. Coltrin, J.F. Grcar, E. Meeks, H.K. Moffat, A.E. Lutz, G. Dixon-Lewis, M.D. Smooke, J. Warnatz, G.H. Evans, R.S. Larson, R.E. Mitchell, L.R. Petzold, W.C. Reynolds, M. Caracotsios, W.E. Stewart, P. Glarborg, C. Wang, O. Adigun, W.G. Houf, C.P. Chou, S.F. Miller, Chemkin Collection, Release 3.7.1, Reaction Design, Inc., San Diego, CA, 2003.
[16] V. Golovichev, available at: http://www.tfd.chalmers.se/~valeri/.
[17] S. Tanaka, F. Ayala, J.C. Keck, Combust. Flame 133 (2003) 467–481.
[18] P.A. Glaude, R. Fournet, V. Warth, F. Battin-Leclerc, G.M. Côme, G. Scacchi, available at: http://www.ensic.u-nancy.fr/DCPR/Anglais/GCR/generatedmecanisms/isooctane.